# Numerical Analyses for Cavitation Surge in a Pump with the Square Root Shaped Suction Performance Curve

Motohiko Nohmi, Satoshi Yamazaki, Shusaku Kagawa, Byugjin An, Donghyuk Kang, Kazuhiko Yokota

# Numerical Analyses for Cavitation Surge in a Pump with the Square Root Shaped Suction Performance Curve

Motohiko Nohmi[1]*, Satoshi Yamazaki[2], Shusaku Kagawa[3], Byugjin An[1], Donghyuk Kang[2], Kazuhiko Yokota[2]

ISROMAC 2016

International Symposium on Transport Phenomena and Dynamics of Rotating Machinery

Hawaii, Honolulu

April 10-15, 2016

**Abstract**

The suction performance curves of the hydraulic pumps show several characteristics such as a sudden drop and gradual decay of pump head and so on. In some particular cases, suction performance curves have a square root shape of "√" that shows a drop followed by a short term rise and another drop of pump head. In the present study cavitation surge under the square root shaped curve is analyzed by using numerical analyses.

Two methods of a lumped parameter system calculation and a distributed parameter system calculation that is in other words three dimensional computation of Navier Stokes Equations are applied. In the case of a lumped parameter system calculation, pump static pressure rise is assumed on the given square root shaped function. Dynamic behaviors of the pump cavitation are represented by the cavitation compliance and the mass flow gain factor. Ordinary Differential Equations are discretized by the second order Runge-Kutta method. In the case of 3D CFD, a commercial code of ANSYS-CFX with cavitation model is adopted.

Intensive cavitation surges are observed from the computed results of both methods. Intensive cavitation surge exists around the operating point at the negative slope part of the suction performance curve in the case of the lumped parameter system calculation. It exists around the operating point at the positive slope part in the case of 3D CFD. Boundary conditions of the computation have significant effects on the characteristics of the cavitation surge.

**Keywords**

Cavitation Surge—Pump—Lumped Parameter Analysis— Square Root Shaped Suction Performance Curve

[1]*EBARA Corporation, Fujisawa-shi Japan*

[2]*Aoyama Gakuin University, Sagamihara, Japan*

[3]*EBARA Corporation, Futtsu-shi Japan*

***Corresponding author**: nohmi.motohiko@ebara.com

## INTRODUCTION

The suction performance curves of the hydraulic pumps show several characteristics such as a sudden drop and gradual decay of pump head and so on. In some particular cases, suction performance curves have a square root shape of "√" that shows a drop followed by a short term rise and another drop of pump head.

The examples of the square root shaped curves are seen in many literatures [1-4]. The authors' group has studied the cavitation surge of the pump with the square root shaped curves by using EFD and CFD [4-6]. It is suggested that the square root shaped curve characteristics might have relations to the cavitation surge of the pumps. The cavitation surge often causes severe noise and vibration on the pipeline system and it would be beneficial for fluid machinery industries to obtain prediction methods of the cavitation surge. The square root shaped curve characteristics could be captured by CFD and its fluid dynamic mechanism has been clarified by degrees [6].

It is supposed that the hydraulic system surrounding the cavitating pump has significant effects on the cavitation surge. The system dynamics of the cavitation surge with the negative slope of the suction performance curves has been already studied by some of the authors by using stability analyses and dynamics in frequency domain [7].The objective of the present study is to analyze and clarify the cavitation surge of the pump with the square root shaped curve from the standpoints of the hydraulic system dynamics in time domain. The final goal of this study is to develop the engineering tools to predict and to prevent any kinds of cavitation instabilities considering the hydraulic system dynamics.

In the present study cavitation surge under the square root shaped curve is analyzed by using numerical analyses. Two methods of a lumped parameter system calculation and a distributed parameter system calculation that is in other words three dimensional computation of Navier Stokes Equations are applied. In the case of a lumped parameter system calculation, pump static pressure rise is assumed on the given square root shaped function. Dynamic behaviors of the pump cavitation are represented by the cavitation compliance and the mass flow gain factor. Ordinary Differential Equations are discretized by the second order Runge-Kutta method. In the case of 3D

CFD, a commercial code of ANSYS-CFX with cavitation model is adopted.

## 1. METHODS

### 1.1 Lumped Parameter System Calculation

Objective pump sysyem is shown in Fig.1 The rotational speed of the pump is assumed constant in this study. The square root shaped suction performance curve of this pump is shown in Fig.2. The governing equations with assumption of incompressible fluid flow are as follow.

$$P_{T1} = \text{const.} \quad (1)$$

$$P_{T2} = \text{const.} \quad (2)$$

$$\rho L_1 \frac{dQ_1}{dt} = S_1(P_{T1} - P_S) - \frac{\lambda_1 \rho L_1 Q_1^2}{2D_1 S_1} \quad (3)$$

$$\rho L_2 \frac{dQ_2}{dt} = S_2(P_P - P_{T2}) - \frac{\lambda_2 \rho L_2 Q_2^2}{2D_2 S_2} \quad (4)$$

where $P$ is static pressure, $Q$ is volume flow rate, $L$ is length of a pipe, $S$ is cross sectional area of a pipe, $D$ is diameter of a pipe, $\rho$ is density of water and $\lambda$ is Darcy's skin friction coefficient respectively. In this study only the skin friction is considered as the resistance in the system however some valves in the pipelines can be modeled by similar manner to the skin friction if necessary. Subscripts of *1* is a pump upstream pipe, *2* is a pump downstream pipe, *S* is inlet of a pump, *P* is outlet of a pump, *T1* is a tank number one and *T2* is a tank number two. Eqs. 3 and 4 are equations of motion of water columns in the pipes upstream and downstream of the pump respectively. In this study volume flow rates upstream and downstream of the pump are assumed not equal.

The pump characteristic including the suction performance is as follows.

$$P_P - P_S = F(Q, P_S) \approx D_{PQ}(Q - Q_0) + F(Q_0, P_S) \quad (5)$$

$$where \quad D_{PQ} = \frac{\partial F}{\partial Q}_{Q=Q_0}$$

In this study pump inlet pressure $P_S$ and static pressure rise of the pump $P_P$-$P_S$ are selected as the suction performance characteristic values instead of conventional NPSH and pump head rise. $F$ is the prescribed function of the square root shaped suction performance curve of static pressure rise as seen in Fig.2. $Q_0$ is the volume flow rate at the initial operating point. $D_{PQ}$ is the slope of the $F$ curve at the initial operating point and is assumed constant in this study. $Q$ in Eq.5 is the instantaneous volume flow rate of the pump and is defined as $(Q_1+Q_2)/2$. $F(Q_0,P_S)$ in Eq.5 is the time averaged suction performance curve. Therefore the pump operating point always moves over the same time averaged curve even if the pump is under the surging situation.

The dynamics of the cavitation inside the pump are modeled as follow.

$$\frac{dV_C}{dt} = \frac{\partial V_C}{\partial P_S}\frac{\partial P_S}{\partial t} + \frac{\partial V_C}{\partial Q_1}\frac{\partial Q_1}{\partial t} = \frac{\partial V_C}{\partial P_S}\frac{dP_S}{dt} + \frac{\partial V_C}{\partial Q_1}\frac{dQ_1}{dt}$$

$$= -K\frac{dP_S}{dt} - M\frac{dQ_1}{dt} \quad (6)$$

$$K = -\frac{\partial V_C}{\partial P_S} \quad (7)$$

$$M = -\frac{\partial V_C}{\partial Q_1} \quad (8)$$

$Vc$ is cavitation volume and $K$ and $M$ are cavitation compliance and mass flow gain factor respectively.

In this study it is assumed that cavitation always exists in the pump. The continuity equation of the fluid in the pump is as follows.

$$Q_1 - Q_2 = -\frac{dV_C}{dt} \quad (9)$$

Following Eq.10 is developed from Eq.6 and Eq.9.

$$\frac{dP_S}{dt} = \frac{1}{K}\left(Q_1 - Q_2 - M\frac{dQ_1}{dt}\right) \quad (10)$$

Equations 3, 4 and 10 are computed in time domain by using the second order Runge-Kutta method. In this study the momentum of the liquid water inside the pump is not considered. The liquid water inside the pump is continuous to the water column in the outlet pipe, and its inertial effect can be involved by modifying Eq.4. This effect shall be evaluated in the next study.

The calculation are carried out for three operating points of A, B and C in Fig.2. The parameters for calculation are as seen in Tab.1.

Table 1. The parameters for lumped parameter calculation

| Parameter | Value | Unit |
|---|---|---|
| $D_1$, $D_2$ | 0.1 | m |
| $L_1$, $L_2$ | 10 | m |
| $S_1$, $S_2$ | $7.85 \times 10^{-3}$ | $m^2$ |
| $\rho$ | 1000 | $kg/m^3$ |
| $\lambda$ | 0.01 | |
| $K$ | $2 \times 10^{-8}$ | $m^3/Pa$ |

The scale of the piping system written in Tab.1 is set supposing the small experimental rig in the laboratory. In this study $K$ is kept constant to the value of $2X10^{-8}$ $m^3/Pa$ that is found to cause a surging with the frequency of a few Hz in preliminary calculation. In this study K and M are given based on the numerical experiments. It should be mentioned that establishing the method to estimate $K$ and $M$ of the objective pump by using experimental results and or CFD results would be essential for the prediction of the surging.

The function of $F$ in Eq.5 is as follows.

$$
\begin{aligned}
F &= 100 \text{ kPa} && : (P_S > 25000\,\text{kPa}) \\
&= 4P_S && : (20000\text{kPa} < P_S \le 25000\,\text{kPa}) \\
&= -2P_S + 120000 && : (15000\text{kPa} < P_S \le 20000\,\text{kPa}) \\
&= 6P_S && : (P_S \le 15000\,\text{kPa}) \qquad (11)
\end{aligned}
$$

where $Q_0 = 7.85 \times 10^{-3}$ m$^3$/s and $D_{PQ} = -1.27 \times 10^{-6}$ Pa s/m$^3$

The value of $Q_0$ is calculated based on the initial flow velocity of 1m/s in the pipe. The value of $D_{PQ}$ is 10% of the pump static pressure rise of 100 kPa divided by $Q_0$. Other parameters are adjusted for each calculation cases.

### 1.2 Distributed Parameter System Calculation

In the design research of the pump impeller the computed suction performance curve with square root shape was observed accidentally. In the present study, the geometry and the operating conditions of this pump impeller was adopted for case study. It should be mentioned that the pump geometry, operating points and the system parameter are different to those for the lumped parameter system analyses. On the preliminary stage of the research, qualitative comparison for lumped parameter analyses and distributed parameter analyses is carried out in this study. The original computation was steady RANS computation with cavitation model by using commercial CFD code ANSYS-CFX. SST k-ω turbulence model and Rayleigh-Plesset cavitation model were used. The computation domain was just limited to the single pitch flow passage of the centrifugal impeller with periodic boundary conditions. Velocity was fixed at the inlet and static pressure was fixed at the outlet for boundary conditions. This impeller was designed for the pump with suction volute. Due to the existence of the suction volute upstream the impeller, there could be the swirl component of the velocities in the impeller inlet flow. Estimated velocity distribution with swirl component was used for the inlet boundary condition in the original steady computation. For the original computation domain, the inlet and outlet are very close to the leading edge and trailing edge of the impeller respectively. As described in the lumped parameter system analyses, the existences of the pipes upstream and downstream of the pump might be important for the system dynamics. Inlet pipe is added to the original computation domain. Exactly same velocity distribution is applied to the inlet of the additional pipe. It is confirmed that the swirl components do not decay in the additional inlet pipe and still exist just upstream of the pump. At the downstream of the pump impeller, a simple diffuser vane and a pipe with rectangular cross section are added. The exit of the downstream pipe is slightly contracted in order to avoid reverse flow. In this study, the dynamics of rotor stator interaction are out of the research scope, so the vane numbers of the impeller and the diffuser are set identical and the frozen rotor approach is used to connect rotor and stator. The objective computation domain is seen in Fig.3.

The element number is about 500 thousand and the node number is about 400 thousand in the whole computation domain. The computation with finer grids could not be carried out due to the limited cpu resources of the present research framework. The grid dependency of the numerical results is important issue and should be examined in the next work.

By adding the inlet and outlet pipes to the original computation domain, the calculation by ANSYS-CFX in this study is equivalent to the lumped parameter calculation for the system in Fig.1. If the physics of $K$ and $M$ are reasonably included in the cavitation model in ANSYS-CFX, the surging computation by ANSYS-CFX could be more accurate compared to the lumped parameter computation, because the complex three dimensional flow characteristics in the pump are considered in ANSYS-CFX.

Before starting the unsteady computation, steady cavitation CFD is carried out again for the modified geometry. The boundary conditions of the steady computation are same for the original computation. The steady computation results are used for the initial conditions of the unsteady computation.

For unsteady computation two cases with different boundary conditions are examined. In the first case, the exactly same boundary conditions for steady computation are used for unsteady computation. In this case volume flow rate at the pump inlet is fixed unlike in the case of lumped parameter system analyses.

In the second case the inlet volume flow rate can be variable. Inlet volume flow rate is changed time step by time step as written in the following procedure [8]. A tank with constant static pressure and a pipe with fixed length are assumed to exist upstream of the 3D computation domain as described similarly in Eq.1 and Eq.3. These lumped parameter analyses are calculated by using ANSYS-CFX user's subroutine and are coupled to the 3D computation through boundary conditions. $P_S$ in Eq.3 is derived from the inlet static pressure of 3D computation domain. Calculated $Q_1$ in Eq.3 is used for the inlet boundary condition of 3D computation domain. Swirl component of the velocity at the inlet for 3D computation is assumed variable proportionally to the inlet volume flow rate, however this swirl component information is not feed backed to the lumped parameter calculation. In Eq.3 for this 3D computation case $L_1$ is 5m fixed and $\lambda$ is zero fixed.

It takes quite long cpu time to compute the cavitation surge with the frequency of a few Hz even for the single pitch calculation of the impeller. While computation, unsteady flow characteristics are monitored. After confirming that the computation result arrives in the final stage such as the stable oscillation, the computation is stopped and the stored data is analyzed.

Static pressure $P_S$ and $P_P$, total pressure $TP_S$ and $TP_P$, volume flow rate $Q_1$ and $Q_2$, cavitation volume $V_C$ and other parameters are normalized and evaluated as written below.

$$
\begin{aligned}
\varphi_S &= P_S / (\rho U^2 / 2) \\
\varphi_P &= P_P / (\rho U^2 / 2) \\
\varphi_{TS} &= TP_S / (\rho U^2 / 2) \\
\varphi_{TP} &= TP_P / (\rho U^2 / 2) \\
H_{norm} &= \varphi_{TP} - \varphi_{TS}
\end{aligned}
$$

$$NPSH_{norm} = (TP_S - P_V)/(\rho U^2/2)$$
$$\sigma = (P_S - P_V)/(\rho U^2/2)$$
$$\phi_1 = Q_1/Q_0$$
$$\phi_2 = Q_2/Q_0$$
$$VC_{norm} = N \times V_C / \frac{\pi D_2{}^2 B_2}{4}$$

For subscripts, *1* is a pump upstream pipe, *2* is a pump downstream pipe, *S* is inlet of a pump, *P* is outlet of a pump in a similar way to the lumped parameter analyses. $P_S$, $TP_S$ and $Q_1$ are specified at the inlet plane and $P_P$, $TP_P$ and $Q_2$ are specified at the outlet plane in Fig.3 respectively. *U* is the tip speed of the rotating impeller trailing edge. $P_V$ is the saturation vapor pressure. $\sigma$ is cavitation coefficient. $Q_0$ is initial volume flow rate used for the inlet boundary condition for steady computation. $D_2$ is the diameter of the pump impeller and $B_2$ is the spanwise length of the trailing edge of the impeller respectively. *N* is the blade number of the impeller.

## 2. RESULTS AND DISCUSSION

### 2.1 Lumped Parameter System Cases

#### *2.1.1 Results at the Point A*

It is assumed that cavitation does exist even on the flat part of the suction performance curve such as Point A in this study. Such situations are not exceptional for suction performance measurements of the pumps. For calculation $P_{T1}$ and $P_{T2}$ are set to 50.5kPa and 149.5kPa respectively. Assuming the equilibrium state, initial values of $P_S$ and $P_P$ are 50kPa and 150kPa respectively. $Q_1$ and $Q_2$ are equal to $Q_0$. Then stepwise perturbation of $Q_1$=1.01 X $Q_0$ is given. Following transient processes are computed. From the preliminary computation *M* is set to 2.55 X $10^{-3}$ s in order to maintain neutral stability. If *M* is specified more than 2.55 X $10^{-3}$ s then numerical results are diverged. *M* less than 2.55 X $10^{-3}$ s ceases oscillation. This means that the oscillation of cavitation surging is damped due to the friction loss in the piping system without appropriate value of mass flow gain factor. Results are seen in Fig.4. After transient process of about 6 s, static pressure change and volume flow rate change at the pump inlet and the outlet show continuous sinusoidal wave of same amplitude and same frequency. The phase difference of inlet and outlet volume flow rate is 180 degrees. Frequency of oscillation is about 1.41Hz. By neglecting *M* and $\lambda$, this frequency can be simply calculated from Eq.3, Eq.4 and Eq.10 as follows.

$$f = \frac{1}{2\pi}\sqrt{\frac{2S_1}{K\rho L_1}} = 1.41 \text{ Hz} \qquad (12)$$

Analytical result and numerical result show good agreement.

#### *2.1.2 Results at the Point B*

$P_{T1}$ and $P_{T2}$ are set to 23kPa and 112kPa respectively. Initial values of $P_S$ and $P_P$ are 22.5kPa and 112.5kPa respectively. Starting process of cavitation surge is exactly same to the case of the surging at the point A. *M* is set to 1.09 X $10^{-2}$ s in order to maintain neutral stability. It takes about 40 seconds to arrive in the final state of oscillation. Results in first five seconds are seen in Fig.5. Qualitative characteristics are similar to the case of the point A, although the amplitude of pressure and volume flow rate at the pump outlet are much higher than those at the inlet. These are due to the highly positive slope of the suction performance curve around the point B as seen in Fig.2. Frequency of oscillation is about 2.44Hz.

#### *2.1.3 Results at the Point C*

$P_{T1}$ and $P_{T2}$ are set to 18kPa and 102kPa respectively. Initial values of $P_S$ and $P_P$ are 17.5kPa and 102.5kPa respectively. Starting process of cavitation surge is exactly same to the case of the surging at the point A. From the preliminary computation it was found that *M* less than 8 X $10^{-2}$ s ensures stable oscillation. Results in first ten seconds with the case of *M*=0 s are seen in Fig.6. It takes about 30 seconds to arrive in the final state of stable oscillation. Result of $P_S$ shows triangular wave. $P_P$ shows more complicated waveform with many peaks. Primary frequency of oscillation is about 1.26 Hz. Compared to the case of point A, pressure and flow rate amplitudes of this case are roughly ten times larger.

Fig.7 shows Lissajous curve of the results in $P_S$ - ($P_P$ -$P_S$) plane. In the case at the point C, the operating point continues transition over positive and negative slope section in the suction performance curve.

### 2.2 Distributed Parameter System Cases

#### *2.2.1 Suction Performance Curves by Steady computation*

Two types of suction performance curves by ANSYS-CFX are shown in Fig.8. In both curves, the square root shaped characteristics are clearly observed. In the computation results cavitation is generated on the suction surface of the blade. In accordance with the lumped parameter system calculations, two operating points of B and C in Fig.8 are selected for the initial conditions of the unsteady computations. Unlike in the case of the lumped parameter system, any artificial perturbations are not applied for unsteady computations. It should be mentioned that Eq.9 is almost satisfied in ANSYS-CFX cavitation computation, however some discrepancy is also observed in the previous study [8]. This situation is also similar in the present study.

#### *2.2.2 Results at the Point B*

Computed results for the case of fixed volume flow rate at the inlet are seen in Fig.9. Oscillation is initiated and grows up intensively. It takes about 3 seconds to arrive in the final state of stable oscillation. Amplitude of volume flow rate at the pump outlet is about 0.5% of the initial volume flow rate. The frequency of the oscillation is about 2.62 Hz. In this case, volume flow rate is fixed and the mass flow gain factor defined in Eq.8 has no effect on the system dynamics, however significant cavitation surge occurs in 3D computation. Further study is required for this issue for developing more accurate lumped parameter model.

Computed results for the case of variable volume flow rate at the inlet are seen in Fig.10. In this case, the operating point shows some transition from the steady computation results with oscillation. The frequency of the oscillation is about 4.3 Hz. Through the transition, the volume flow rate increases up to about 0.4% and the static pressure rise increases up to about

0.7%. After the transition, the oscillation is diminished. This result is similar to the lumped parameter analysis result with insufficient value of mass flow gain factor.

Although the same initial conditions and same numerical scheme, the difference of the boundary conditions results in totally different characteristics of the system dynamics of cavitation surging. The stable oscillation of the fixed inlet volume flow rate case is not well understood. Further study would be necessary to clarify these mechanisms.

#### *2.2.3 Results at the Point C*

Computed results for the case of fixed volume flow rate at the inlet are seen in Fig.11. The results show clear oscillation with frequency of about 1.48Hz. Compared to the case of Point B, the cavitation surging is much weaker. Amplitude of volume flow rate at the pump outlet is about 0.07% of the initial volume flow rate. The inlet static pressure change shows triangular waveform.

Computed results for the case of variable volume flow rate at the inlet are seen in Fig.12. The frequency of the oscillation is about 2.52 Hz. Amplitude of volume flow rate at the pump outlet is about 0.18% of the initial volume flow rate. At the inlet both static pressure change and the volume flow change show sinusoidal waveform. On the other hand, pressure and volume flow rate change show more complicated waveform.

Fig.13 shows Lissajous curve of the results in PS - (PP -PS) plane. In the case at the point B, the operating point does not move on the suction performance curve based on the steady computation. This suggests that the basic assumption for lumped parameter system analyses of the operating point stuck on the suction performance curve might not be always correct in the real situation of the cavitation surge. Unlike in the case at the point C of the lumped parameter analyses, the moving range of the operating point around the point C is very narrow.

## 3. CONCLUSIONS

In the present study cavitation surge with the square root shaped suction performance curves are analyzed by using numerical analyses. Two methods of a lumped parameter system calculation and a distributed parameter system calculation that is in other words three dimensional computation of Navier Stokes Equations are applied. By using both methods, cavitation surge could be calculated, however qualitative discrepancies are observed between two method results. It was also found that the boundary conditions for three dimensional calculations have significant effects on the computed results of the cavitation surge.

In further study, more accurate model of pump characteristics under cavitation surge would be required for the lumped parameter calculation. Reliable calculation method of cavitation compliance and mass flow gain factor from both three dimensional cavitation CFD and experimental results should be established. Based on the three dimensional CFD, detailed observation of unsteady characteristics of cavitating flow inside a pump under cavitation surge is also necessary.

## ACKNOWLEDGMENTS

The authors would like to express their sincere gratitude to Professor Mehdad Zangeneh of University College London and his colleagues at Advanced Design Technology for finding the calculated result with square root shaped suction performance curve through numerous computations of ANSYS-CFX. The authors also would like to express their sincere thanks to Mr. Takayuki Sakai for his contribution to the complex calculations of ANSYS-CFX.

## REFERENCES

[1] K. Kamijo and A. Suzuki. An experimental investigation of flat-plate helical inducers for rocket turbo pumps. *Technical Report of National Space Laboratory*, TR-345, 1973. in Japanese

[2] T. Kimura, M. Shimagaki and Y. Yoshida. CFD simulation of cavitating flow in turbopump inducer. *Proc. 12th Symposium on cavitation*, 61–64, 2004, in Japanese

[3] O.Coutier-Delgosha, G. Caignaert, G. Bois, J.-B. Leroux. Influence of the Blade Number on Inducer Cavitating Behavior. *J. Fluids Eng. ,ASME*,Vol.134 081304, 2012, in Japanese

[4] S. Hatano, D. Kang, S. Kagawa, M. Nohmi, and K. Yokota. Study of Cavitation Instabilities in Double-Suction Centrifugal Pump. *International Journal of Fluid Machinery and Systems*, Vol.7 No.3, 94-100, 2014

[5] M. Nohmi, S. Kagawa, B. An, D. Kang, S. Hatano, and K. Yokota. A Lumped Parameter System Analysis for Cavitation Surge in a Pump with the Square Root Shaped Suction Performance Curve. *Proc. 17th Symposium on cavitation*, 2014, in Japanese

[6] S. Yamazaki, D. Kang, S. Kagawa, B. An, M. Nohmi, and K. Yokota. Study of Square Root Characteristics in a Double-Suction Centrifugal Pump. *Proc. AICFM13*, AICFM13-200, 2015

[7] D. Kang, S. Hatano, and K. Yokota. One-Dimensional Analysis of Cavitation Surge with a Hydraulic System. *Proc. 16th Symposium on cavitation*, 2012, in Japanese

[8] M. Nohmi, T. Ikohag and Y. Iga. On Boundary Conditions for Cavitation CFD and System Dynamics of Closed Loop Channel. *Proc. AJK2011-FED*, AJK2011-33007, 2011

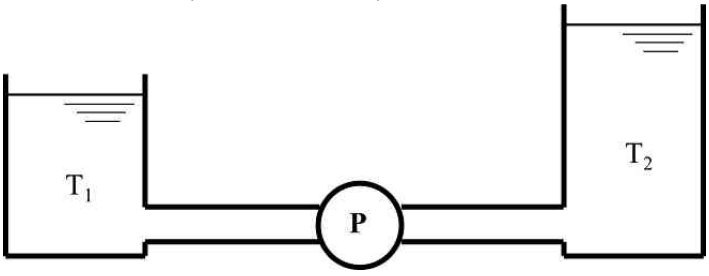


Fig.1 Objective Model of a Pump System

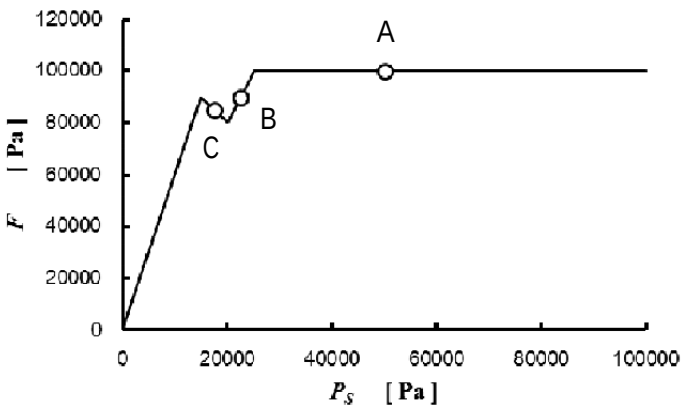


Fig.2 A Square Root Shaped Suction Performance Curve ($Q=Q_0$)

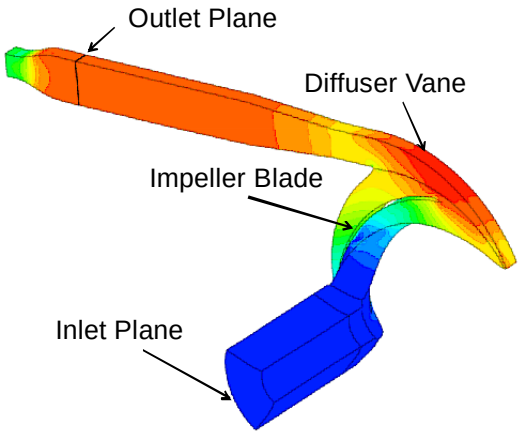


Fig.3 Computation Domain of the Distributed Parameter Calculation by ANSYS-CFX

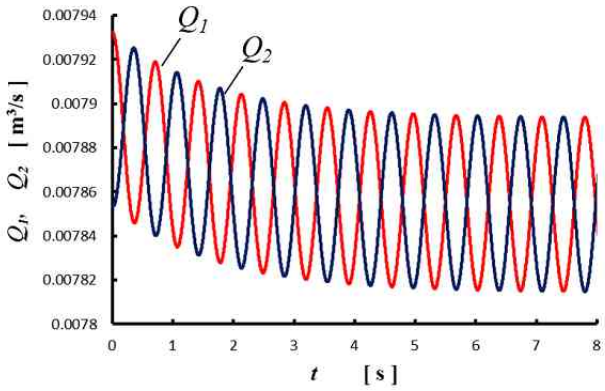


(a) Time History of Volume Flow Rate

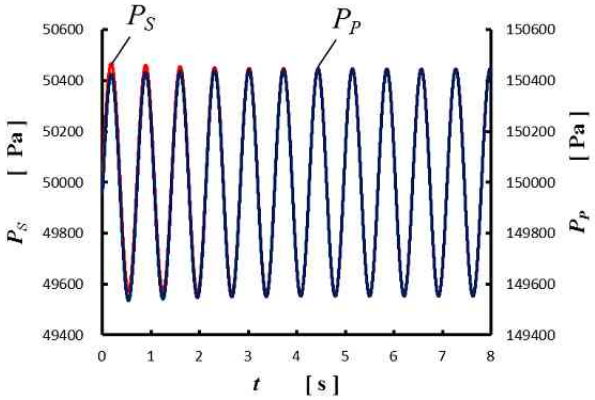


(b) Time History of Pump Static Pressure

Fig.4 Computed Results of the Point A

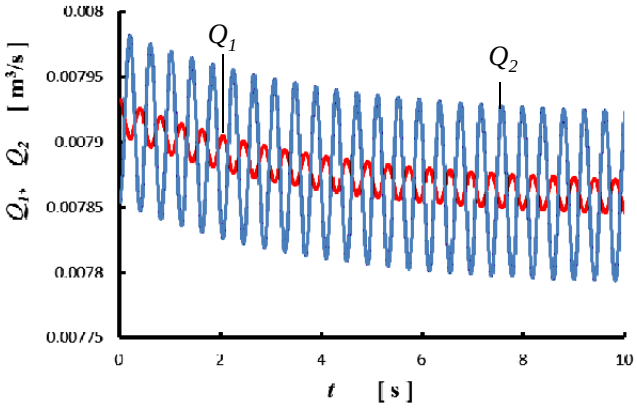


(a) Time History of Volume Flow Rate

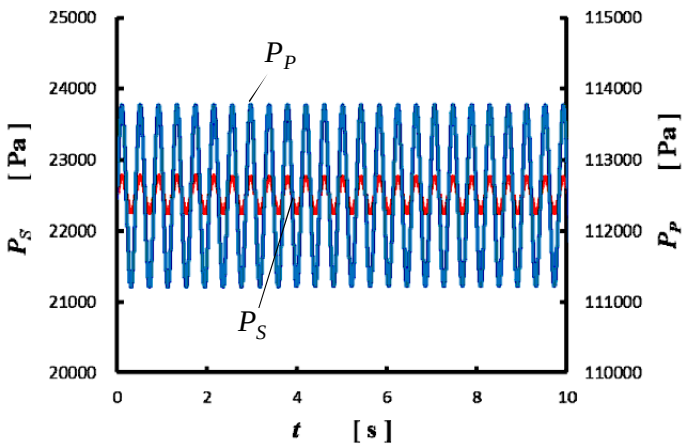


(b) Time History of Pump Static Pressure

Fig. 5 Computed Results of the Point B

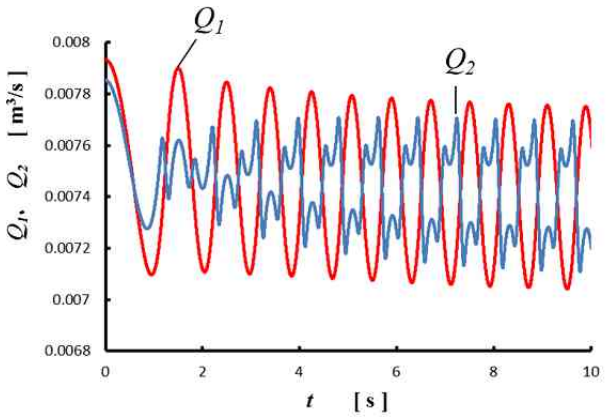


(a) Time History of Volume Flow Rate

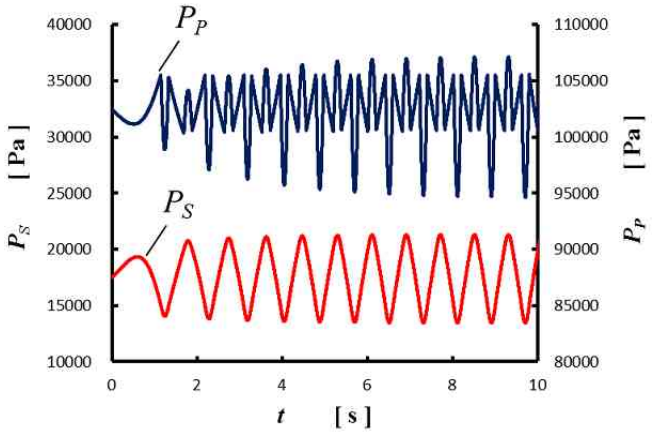


(b) Time History of Pump Static Pressure

Fig.6 Computed Results of the Point C

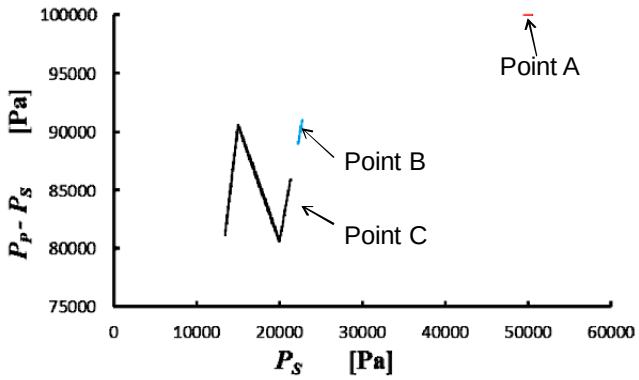


Fig.7 Lissajous Curve of Cavitation Surge

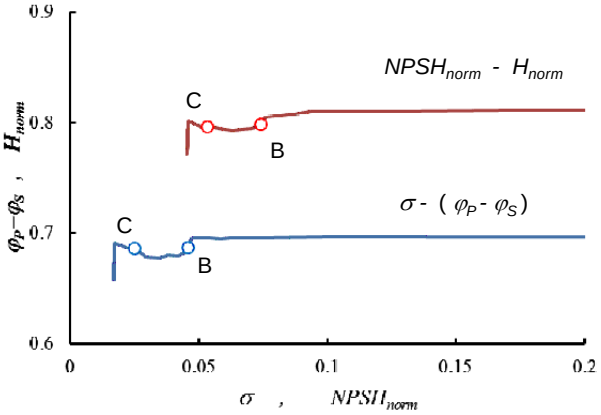


Fig.8 Computed Suction Performance Curves

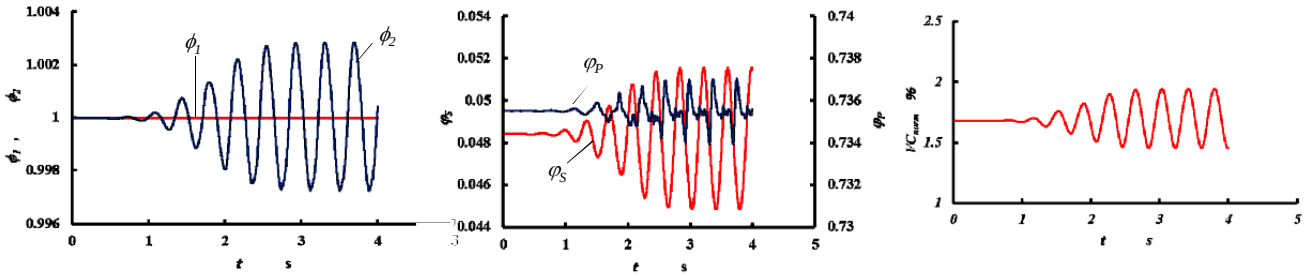


(a) Time History of Volume Flow Rate (b) Time History of Pump Static Pressure (c) Time History of Cavitation Volume

Fig.9 Computed Results of the Point B with Fixed Volume Flow Rate at the Inlet

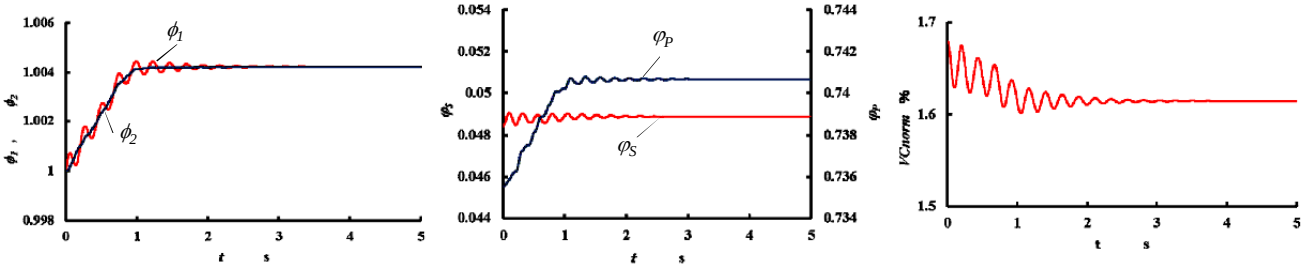


(a) Time History of Volume Flow Rate (b) Time History of Pump Static Pressure (c) Time History of Cavitation Volume

Fig.10 Computed Results of the Point B with Variable Volume Flow Rate at the Inlet

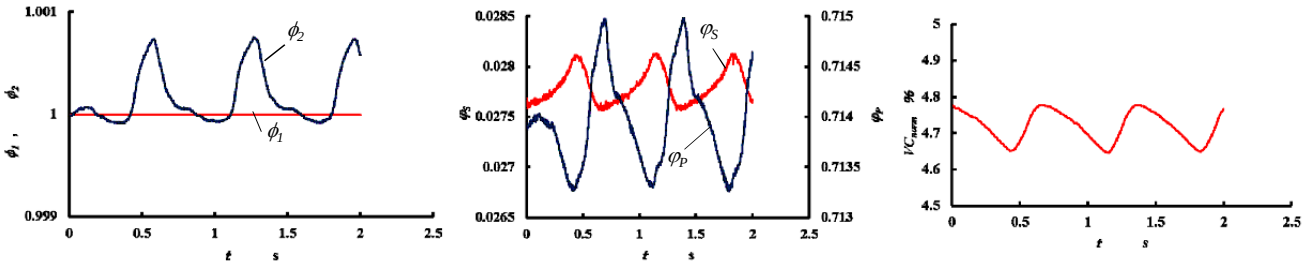


(a) Time History of Volume Flow Rate (b) Time History of Pump Static Pressure (c) Time History of Cavitation Volume

Fig.11 Computed Results of the Point C with Fixed Volume Flow Rate at the Inlet

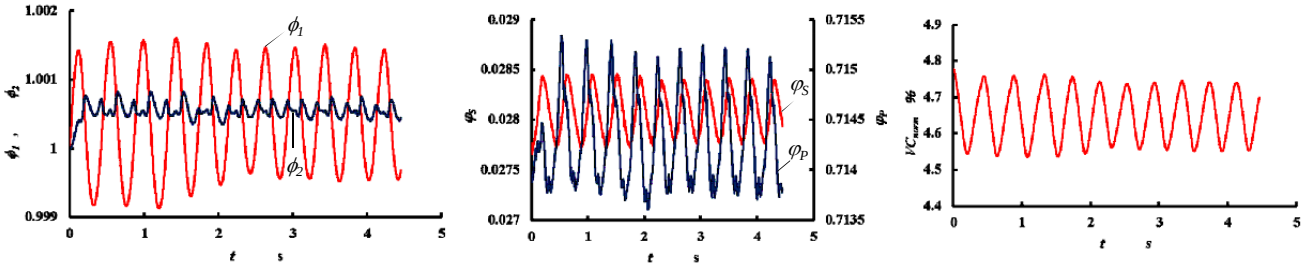


(a) Time History of Volume Flow Rate (b) Time History of Pump Static Pressure (c) Time History of Cavitation Volume

Fig.12 Computed Results of the Point C with Variable Volume Flow Rate at the Inlet

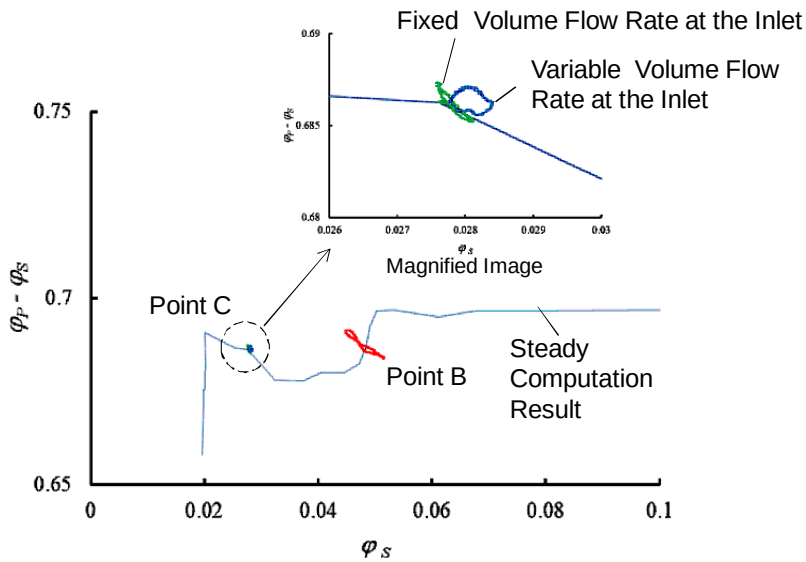


Fig.13 Lissajous Curve of Cavitation Surge